Published in final edited form as:
Lasers Surg Med. 2009 August ; 41(6): 442–453. doi:10.1002/lsm.20782.

Wide-Field Spatial Mapping of In Vivo Tattoo Skin Optical Properties Using Modulated Imaging

Frederick R. Ayers[1,*], **David J. Cuccia, PhD**[2], **Kristen M. Kelly, MD**[3], and **Anthony J. Durkin, PhD**[1]

[1]University of California–Irvine, Beckman Laser Institute, Irvine, California 92612

[2]Modulated Imaging, Inc., Irvine, California 92612

[3]University of California–Irvine, Dermatology, Irvine, California 92612

Abstract

Background and Objectives—Modulated imaging is a new modality capable of wide-field, spatially resolved measurement of in vivo optical properties. Based on spatial light modulation, the method is inexpensive, non-contact, and allows spatial mapping of tissue absorption and reduced scattering coefficients at any wavelength between 450 and 1,100 nm. Currently, clinicians rely on qualitative visual inspection to guide parameter selection for laser-based tattoo removal. MI provides quantitative measurements of multi-colored tattooed skin which may help guide treatment and objectively assess response.

Study Design/Materials and Methods—We have measured the spatially varying optical properties of multicolored tattooed skin over a 50 mm × 50 mm field of view at wavelengths ranging from 650 to 970 nm using MI. These measurements were compared to a similar field of view of non-tattooed skin from an adjacent area.

Results—We have determined the differentiated optical properties in vivo of multi-colored tattooed skin versus non-tattooed skin.

Conclusions—MI provides spatially resolved quantitative information with potential for quantitative assessment of response to treatment and may provide guidance for laser tattoo removal in the future.

Keywords

spectral imaging; tattoo characterization

Introduction

Once practiced by a small portion of society, skin tattooing has become more common place. A recent survey suggests that one in four Americans has at least one tattoo [1]. Following this growth in the practice of tattooing has been an increase in demand for laser tattoo removal. The same survey estimated that 17% of those with a tattoo had considered removing it. The standard of care for tattoo removal involves the use of one of four, or a combination of, Q-switched lasers operating at wavelengths of 532, 694, 755, and 1064 nm. While laser tattoo removal has been effective, it is often an expensive and time-consuming process. Amateur tattoos often require four to six sessions to affect near complete erasure. Professional tattoos,

*Correspondence to: Frederick R. Ayers, Beckman Laser Institute, 1002 Health Sciences Rd, Irvine, CA 92612. fayers@uci.edu.

which use more robust pigments and are generally placed at higher concentrations in the dermis, require an average of 8–12 treatments. In both cases treatments are typically spaced over 4–8 weeks [2,3]. Complications include skin scabbing or blistering due to excessive absorption of laser energy by the surrounding tissue, hypo and hyper pigmentation, and spontaneous tattoo darkening due to the presence of titanium dioxide or ferric oxide [2,4,5]. Ideally, treatment will remove the tattoo with the fewest number of sessions while minimizing these complications. Currently, laser wavelength selection, as well as other parameters such as fluence, is chosen by the clinician based on qualitative observation and previous clinical experience.

The majority of literature involving laser tattoo removal effectiveness has been based on clinical case studies of treatments; however, access to objective information related to tattoo composition, such as optical properties, may provide an avenue with which to improve the efficiency of the treatment. In the mid 1990s, Haedersdal et al. measured the spectral reflectance of tattooed skin from 300 to 800 nm to establish ranges of maximum absorption for several colors. Thirteen tattoos involving fourteen different colors, the most common being red and green, were included in the study [6]. The authors suggested that spectral reflectance information could be used to guide laser selection, but this study did not separate scattering and absorption in the reflectance measurements. Without separating the effect of reduced scattering in the diffuse reflectance values, the accuracy of the absorption values is compromised [7,8]. Also, there is likely usable clinical information contained in the reduced scattering values. Baumler et al. [9] used a spectrophotometer over the wavelengths of 320–1,100 nm to measure the absorption spectra of 41 commercially available pigments suspended in solvent. More recently, Beute et al. [10] performed similar in vitro spectral analysis on 28 common tattoo pigments which were mixed with agar. While providing helpful information for common pigments, this is not a practical method for guiding laser tattoo removal because of the potential for an even larger number of dyes available. Colors in a tattoo are often a combination of pigments chosen by and known only to the original tattoo artist. Also, bench top spectroscopy does not provide information about the in vivo distribution of pigment, nor does it provide reduced scattering coefficient or the optical properties of the underlying skin. On a different tack, O'goshi et al. [11] used confocal scanning laser microscopy to visualize the particle size and density of a tattoo. While this technique is useful for documenting some of the microscopic features of tattoos, this technology is limited in so far as it scans at a single wavelength and cannot provide rapid wide-field characterization of spectral properties.

In this article, we present a new technique, known as modulated imaging (MI) that may be useful for clinical characterization of tattoo pigment prior to tattoo removal. MI is a spatially resolved, non-contact imaging modality based on diffuse optical spectroscopy (DOS) principles which can provide quantitative absorption and scattering contrast of superficial in vivo tissue. In this article, we have applied MI to several multi-colored tattoos. Using MI, we demonstrate that we are able to distill macroscopic reflectance images into spatially resolved maps of optical properties. In addition, we are able to render absorption and reduced scattering spectra between 650 and 970 nm, from different regions of these tattoos.

Materials and Methods

MI is a new wide-field spectral imaging modality that relies on measurements, acquired by a CCD camera, of diffuse reflectance in the spatial frequency domain to deduce the absorption coefficient and the reduced scattering coefficient on a pixel by pixel basis [12]. Additionally, by incorporating a filter wheel or liquid crystal tunable filter into the data acquisition, 2-D optical property maps can be rendered at multiple wavelengths. The first row of Figure 1a shows a stylized field of view imaged by MI when illuminated with planar light (Frequency 0). We also commonly refer to this as “DC illumination.” Below this row, are samples of the image with increasing spatial frequency patterns projected onto the field of view (Frequencies

1 and 2). Each frequency is imaged three times with a 120° phase shift between images to completely tile the field of view. By combining the three phase-shifted illumination images, the signal can be demodulated into maps of frequency dependent diffuse reflectance for the field of view and are graphically represented in Figure 1b. This phase shift and demodulation scheme is not unique to MI and is described in the literature [13,14]. Using tissue simulating liquid phantoms, Cuccia et al. [12] demonstrated the frequency dependent diffuse reflectance is directly related to the wavelength dependent absorption and scattering coefficients and this relationship could be solved analytically using the diffusion approximation or numerically using a Monte–Carlo simulation. Due to the limitations of the diffusion approximation when interrogating highly absorbing tissue, results presented here were solved numerically [12,15]. The work that we describe here is the first published in vivo data using MI. All data were acquired in the Beckman Laser Institute medical clinic under a protocol reviewed by the UC Irvine Investigational Review Board.

A MI system based on Figure 2 was employed for a series of tattoo measurements and is the standard research system employed by the lab to carry out functional studies of in vivo tissue. The near-infrared regime is particularly suited to measurements of endogenous chromophores including oxy, deoxy hemoglobin concentrations and water fraction. The system itself was designed for a myriad of studies including longitudinal studies of cancer progression in preclinical animal models, surveillance of reconstructive tissue flaps, and functional brain imaging in preclinical animal models. Broadband light was generated with a Newport Corporation power source (Newport Corporation, Irvine CA) and a 250 W Tungsten lamp. This light was used to illuminate a DLP Developers Kit 1,024 × 768 pixel digital micro-mirror device (Texas Instrument, Dallas, TX) which spatially modulated the light to be projected. Frequency patterns for the spatial modulation were generated using the sine function in Matlab (The MathWorks, Natick, MA) and sent to the projection device via PowerPoint (Microsoft Corporation, Redmond, WA) as controlled by LabVIEW 7.1 (National Instruments, Austin, TX). The patterned light was projected directly onto the subject's skin approximately 300 mm from the projector system and at approximately a 10° angle to the detection camera. Distance from the system and location of the field of view was maintained with a simple metal frame built with optic post assemblies (Thorlabs, Newton, NJ) which is not shown in the diagram.

Reflected light images were acquired with a Nuance Multispectral Imaging System (CRi, Inc., Woburn, MA) which consists of a liquid crystal tunable filter capable of acquiring at discrete wavelengths (10 nm bandwidth) between 650 and 1,100 nm and a 1,040 × 1,392 pixel, front illuminated CCD camera. Camera-based four by four binning of pixels was employed to optimize the signal-to-noise ratio of the CCD. Interrogating subsurface features with light is inherently lower resolution so our measurements are not negatively affected by the choice to bin [12,16]. With polarizers incorporated into the optics of the camera and the projection system, we were able to cross-polarize the light to reject specular reflection from the skin. Images were saved as TIFF images to the laptop computer for post-acquisition processing. The field of view of the MI system is scalable, but for this study was 50 mm × 50 mm. Measurements were taken at four spatial frequencies, one unmodulated, zero frequency plus three progressively higher frequencies, and spectrally every 20 nm from 650 to 990 nm. The acquired wavelength range was limited by the hardware of the MI system outlined above. Spectral reflectance images were calibrated for system response using a 96 mm × 96 mm × 10 mm tissue simulating phantom having known optical properties (μ_a = 0.0188 mm^{-1} and μ_s'=1.098 mm^{-1} at 650 nm). This is a polydimethylsiloxane (PDMS) phantom and incorporates India ink as an absorber and TiO_2 as a scattering agent [17]. Spectral absorption and scattering coefficients of the calibration phantom were verified using a two-distance frequency domain photon migration (FDPM) measurement which is a self-calibrating measurement [18].

While a number of fitting methods can be employed to extract the absorption and scattering coefficient, we have found that a lookup table method based on the results of "White" Monte–Carlo simulation provides rapid computation with acceptable accuracy [12,19]. Using this method, modeled diffuse reflectance values for each of two spatial frequencies are generated for a population of absorption and reduced scattering combinations. By intersecting the two distinct sets of spatial frequency dependent reflectance values, a lookup table can be generated, a subset of which is graphically represented in Figure 3. A continuum of absorption values (μ_a) and reduced scattering values (μ_s') have been overlaid onto a plot of diffuse reflectance values for spatial frequency 1 on the horizontal axis and spatial frequency 2 on the vertical axis. Intersections on this overlay represent unique absorption and reduced scattering combinations and are located on the larger graph at the values of diffuse reflectance for the chosen frequencies. For the purpose of processing real data, measurements of diffuse reflectance, scaled to the properties of the calibration phantom, at each spatial frequency are used to rapidly look up the proper absorption and scattering combination as shown in this graph. This processing is done in Matlab and employs the *griddata* function. In the article by Cuccia et al. [12], a similar approach was shown to accurately deduce optical properties of homogeneous liquid phantoms over a wide range of optical properties, with recovered values deviating by less than 10% from expected reduced scattering values and less than 15% from expect absorption values. All data processing and analysis were done on a Windows Professional 64-bit Edition desktop running a dual-core 3 GHz Pentium D processor.

The advantages in computation speed for this scheme are highlighted when we compare the processing time between the lookup-table based process and an iterative, least-squares based method. To deduce the average optical properties of a small, 3.7 mm × 4 mm, 21 × 23 pixel region of normal skin, the iterative process requires 2 hours to compute solutions while the lookup-table based process required 6 minutes. This efficiency is essential for the larger field-of-views used in this study. Additionally, the lookup table does not require an initial guess of optical properties which is advantageous when dealing with the large dynamic range of optical properties between normal and multi-colored tattooed skin. Typical non-tattooed skin will have optical properties in a tight range of values [20]. A lookup table needs only to be created using an absorption and scattering set large enough to capture the appropriate in vivo values. However, because the absorption and scattering coefficients of tattooed skin have not been fully characterized, we have attempted to capture a much larger range of optical properties in our lookup table which is outlined in Table 1. The ability to accurately determine absorption and reduced scattering coefficient based on a two frequency look-up table relies on the relative decrease in contrast to absorption versus reduced scattering as the frequency increases The first frequency was always a frequency of zero, which corresponds to broad area uniform illumination, and is typically the frequency that is most sensitive to the absorption coefficient [12]. The second frequency used for the look-up table was kept above 0.16 cycles per mm which has less sensitivity to absorption versus wavelength, but is sufficiently sensitive to scattering so that absorption is easily separable from reduced scattering coefficient.

In this article, we present MI results obtained for three tattoos from separate volunteers. Figure 4 shows digital color photographs for each of the three tattoos and the boundaries of the measurement field of view. The first subject (Fig. 4a) was a 29-year-old Caucasian female with a 6-year-old tattoo on her right shoulder blade. The second subject (Fig. 4b) is a 30-year-old Hispanic male with a 14-year-old tattoo on his upper, left arm. The third subject (Fig. 4c) is a 20-year-old Caucasian female with a 1-year-old tattoo located on her right shoulder blade.

Results

Figure 5 shows the average optical properties for a selected region of non-tattooed skin on each subject. For each graph shown, the *solid line* corresponds to data from subject #1 (tattoo

depicted in Fig. 4a), the *dotted line* corresponds to data from subject #2 (tattoo depicted in Fig. 4b), and the *broken dashed line* corresponds to data from subject #3 (tattoo depicted in Fig. 4c). All three regions demonstrate absorption spectra with elevated absorption values in the visible portion of the wavelength spectrum and at the long wavelength end of the spectrum as the first water peak is approached. As expected, data from the subject with the clinically least pigmented skin (Fig. 4a) shows the lowest absorption values and data from the subject with the clinically darkest skin (Fig. 4b) shows the highest absorption values. The second graph in the figure shows the average reduced scattering coefficient, which is similar for each subject.

Figure 6 plots the average broadband diffuse reflectance, average absorption coefficients and average reduced scattering coefficients versus wavelength of three differently colored tattooed regions of interest, as well as a region of non-tattooed skin, for the first subject (Fig. 4a). This is a tattoo of a sunflower and features green, red-orange, and burnt-red colors. We have selected regions of interest corresponding to each of these colors to highlight the ability of MI to differentiate between them in the near-infrared spectrum. Looking to the graph of absorption versus wavelength, (Fig. 6c) the *solid line* corresponds to the region of normal skin. The absorption features seen in Figure 5 above cannot be seen here because of the expanded scale needed to capture the range of absorption observed for the tattooed skin, which are several orders higher in magnitude than for normal skin. The *dotted line* corresponds to a green region of the tattoo and features a large, downward sloping spectrum as we move from 650 to 870 nm which includes the visible red spectrum and the start of the near-infrared spectrum. The *dashed line* corresponds to a red-orange portion of the tattoo. As expected, this region of interest shows significantly lower absorption values in the 650–870 nm range of the spectrum, but is still several orders higher than that of non-tattooed skin. The *broken dashed line* corresponds to a burnt-red portion at the center of the sunflower. This area is the darkest portion of the tattoo in terms of clinical appearance and our MI data indicate that this region contains high absorption values throughout the measured near-infrared spectrum. While the absorption values for each of the selected regions of interest are all significantly higher than that of non-tattooed skin, we can see in Figure 6d, the graph of reduced scattering coefficient versus wavelength, that scattering in the tattooed skin remains on the same scale as non-tattooed skin. The suppressed values relative to those of non-tattooed skin for the scattering coefficient of the *dotted line* and *dashed line* are not true values and are related to scattering versus absorption cross-talk in the homogenous model that occurs at higher levels of absorption. Similar reduced scattering spectra are observed in the second tattoo discussed below. In both cases this cross-talk is witnessed when absorption values exceed 0.1 mm^{-1}. This effect is not seen in the third tattoo where the absorption values never exceed 0.1 mm^{-1}. Of particular interest in Figure 6d is the *dashed line*, again corresponding with the red-orange portion of the tattoo, which demonstrates a higher reduced scattering coefficient than that measured for non-tattooed skin of the same subject. While not confirmed histologically, this increase in scattering suggests the possibility of the presence of TiO_2, a common ingredient in the brighter tattoo colors such as orange [21].

Results obtained for the second subject (Fig. 4b), are presented in Figure 7 which is analogous to Figure 6. For this MI measurement, the field of view is a portion of a large green leaf tattoo. We have selected regions of interests which allow us to look at a green portion of one of the leaves (*dotted line*), blue shading outside of the leaf (*dashed line*), and a portion of non-tattooed skin (*solid line*). Again, the spectral absorption features in Figure 7c of the normal skin have been de-emphasized due to the larger scale required to capture the range of absorption values of the tattooed skin. For the green portion of the tattoo represented by the *dotted line* on the absorption graph, we see a spectrum similar in shape and size to that recorded in Figure 6c, which is also a region of green tattoo. The blue shading introduces a new spectral shape for the absorption coefficients (*dashed line*). For this blue pigmented area, we have extracted even higher values of absorption coefficient and a steeper fall off of values for the tail end of the

visible red spectrum than was observed for the green tattooed region of skin. Farther into the near-infrared spectrum, the blue section shows lower absorption values. Again, the scattering values shown in Figure 7d for tattooed skin are on the same order of magnitude as non-tattooed skin.

Finally, we present data from the third tattoo (Fig. 4c) which features two hands reaching toward each other across a yellow and orange sun. We have selected regions of interest corresponding to yellow (*dotted line*) and orange regions (*dashed line*), as well as normal skin (*solid line*). The spectral plots of diffuse reflectance, absorption coefficient, and reduced scattering coefficient can be seen in Figure 8. Again, the trend of high absorption values (Fig. 8c) for the tattooed region relative to the non-tattooed region continues. Because the yellow portion of the tattoo appears to be a brighter shade than the orange portion of the tattoo, it might be assumed that a yellow tattoo (*dotted line*) would be less absorbing than an orange tattoo (*dashed line*). However, we see that for this particular tattoo that the opposite is true. Additionally, by comparing the optical properties of the region of non-tattooed skin and the region of orange tattoo, we can see that while the diffuse reflectance (Fig. 8b) is similar for both regions of interest, the absorption (Fig. 8c) and reduced scattering (Fig. 8d) coefficients for both areas is substantially different. When compared to non-tattooed skin, the orange tattoo's recovered reduced scattering coefficient is balanced by its higher absorption coefficient resulting in similar reflectance spectra. Again, the elevated reduced scattering value (Fig. 8d) in the orange section may be an indicator that the orange pigment contains a scattering agent such as TiO_2. This demonstrates one of the advantages of the MI system over a simple reflectance measurement that does not separate absorption from scattering.

While average optical properties for an area of tissue are helpful in certain circumstances, Figures 9 and 10 illustrate a different way to look at the optical properties of tissue which harnesses the imaging ability of our technology. Using the leaf tattoo from subject #2 as an example, Figure 9 shows four 221×294 pixel false color, grayscale maps of the absorption coefficient at each pixel in the selected field of view. Each pixel represents a 4×4 binned pixel area of the CCD, and each of the four maps represents the absorption at a different wavelength. This mapping reveals spatial heterogeneities within the measured tissues and is easily observed in tattooed skin. The accompanying histograms illustrate the distribution of absorption coefficients in the field of view. For each wavelength map, the most frequent histogram value occurs near the value of the mean absorption coefficient of the non-tattooed skin. We can see that the range and frequency of higher absorption coefficients is larger on the shorter wavelengths (650 and 750 nm) where the green portion of the tattoos is most absorbing. The maximum value of absorption at the far right of the histograms for wavelengths 650, 750, and 850 nm (designated as white on the false-color maps) is not a true optical property of the tissue and represents an absorption value greater than can be deduced by our measurement system. These values correspond to the black pigment in the tattoo.

Figure 10 repeats the 2-D false color, grayscale map of the green leaf tattoo for the reduced scattering coefficients. These maps present a less varied color distribution, which is predicted above in the average reduced scattering values. Looking to the accompanying histograms, the highest frequency values occur near the mean reduced scattering coefficient of the non-tattooed skin. The distribution of values below the peak represents the suppressed reduced scattering generated by the model that was previously discussed. This effect is most pronounced in the histograms related to the wavelengths of 650 and 750 nm, while the histograms related to the wavelengths of 850 and 950 nm show significantly fewer counts below the mean reduced scattering value. These higher wavelength maps show very high uniformity in color. Again the highest reduced scattering values depicted in white on the maps are caused by absorption values greater than can be deduced by our measurement system. By looking at the extreme values of

both absorption and reduced scattering together, it is easy to recognize these as corresponding to regions of black pigment.

Discussion

Tattoos presented here were all untreated and subjects were not enrolled in a tattoo removal program. Future work in this area will involve volunteers who are seeking laser tattoo removal. This will allow for a longitudinal study of the response to therapy. Additionally, access to a pool of subjects undergoing tattoo removal will enable an investigation of the predictive ability of MI to guide wavelength selection for treatment, or the potential to provide dosimetry guidance to the clinician based on the optical properties of the native skin. While our current results demonstrate the ability of MI to provide relevant information for the purpose of laser tattoo removal, this longitudinal study will better guide discussion of the appropriate insertion point of this technology into the therapeutic process. Also as noted in the Materials and Methods Section, we used an established MI instrument which was optimized for 650 to 970 nm wavelength range. Additional studies should incorporate wavelengths near the operational wavelengths of the single and double frequency Nd:YAG lasers, those most commonly utilized for tattoo removal. This will require an MI instrument that also measures the visible spectrum to at least 532 nm as well as capturing 1,064 nm.

Both absorption and reduced scattering contribute to diffuse reflectance. Because of this, an unknown change in the reduced scattering coefficient could obscure a change in absorption that may not be recognized either visually or through a simple diffuse reflectance measurement. This is a particular strength of MI. As previously implied in the results obtained from yellow and orange regions of the tattoos imaged here, MI can provide information related to the reduced scattering coefficient that is not easily discerned based on clinical appearance. Titanium dioxide and ferric oxide are two scattering agents that are often used in tattoo dyes in order to render certain colors more vibrant. Both of these agents are troublesome for laser tattoo removal as they are not dispersed like the dyes themselves and instead may blacken in response to high intensity laser energy, leaving discoloration to the treated skin rather than improved cosmesis [5]. Currently, when the presence of these agents is suspected, the therapeutic laser is test fired onto a point of the tattoo in question. Presence is then confirmed if the region darkens. Obviously, the ability to a priori determine the presence of these agents has the potential to benefit both the patient and the treating professional.

In this article, we have highlighted the complexities of MI in order to properly introduce the technology. However, as the technique is optimized and reduced to clinical practice, we expect that the underlying process will be transparent to the end user and provide an acquisition and processing experience similar to other simple reflectance techniques while providing the additional information of separated absorption and reduced scattering coefficients. For example, data acquisition time for this set of investigations was in the 10- to 15-minute range. Because this was our first set of in vivo investigations, the emphasis has been on collecting complete spectra over the 650–990 nm range. Consequently, seventeen wavelengths were acquired at four different frequencies at 256×256 binned pixels resulting in 144 Mb of data. However, only two frequencies are required to extract the absorption and reduced scattering coefficient at a given wavelength. Thus, acquisition times can be dramatically reduced by reducing the number of wavelengths to four wavelengths near those of the four therapeutic lasers and acquiring at only the required two frequencies. Additionally, because the novelty of this process exists in the processing algorithms rather than the equipment, the system can be made with consumer grade components ensuring an economical price point.

Future work will also benefit from improved light models for the MI data analysis. While we currently are able to show excellent contrast among highly absorbing regions of tattooed skin,

we have observed that the absorption coefficients are overestimated for absorption coefficients above 0.10 mm^{-1}. This leads to cross-talk between the absorption value and the reduced scattering value, which is underestimated. This is a result of employing a homogenous light transport model to a non-homogenous, layered tissue system. Tattoo ink particles are not uniformly distributed in the skin; instead they are concentrated at the epidermal/dermal interface. Because this layer is several orders of absorption higher than the native tissue, the layer problem is likely exaggerated and can be seen in the figures above. Nevertheless, results obtained using a homogenous model are still illuminating in many cases. At the same time, we are actively working to incorporate a two-layer light transport model into the analysis [22] and expect that the currently observed upper absorption limits are not the absolute limits of the method. Conversely, Cuccia et al. [12] showed that MI could accurately determine absorption coefficients well below the values we have shown for non-tattooed skin.

Conclusions

In this article, we have reported the first set of in vivo results that we have obtained with the MI instrument in the near-IR spectrum, evaluating both non-tattooed and tattooed skin. Results for normal, non-tattooed skin were consistent with those reported elsewhere [20]. Additionally, we were able to determine absorption coefficient values up to ten times higher than the absorption of non-tattooed skin while still being able to quantitatively separate reduced scattering and exhibit the flexibility of our system. Results are presented both as average optical properties and as spatially resolved property maps effectively covering a tissue area of 5 cm × 5 cm. This ability to simultaneous measure a scalable area of tissue is a primary strength of this system when compared to point source-detector technologies. The ability to separate scattering and absorption over a wide-field plane has potential for guiding wavelength selection for tattoo removal and may improve treatment success.

Acknowledgments

This work was supported by the Laser Microbeam and Medical Program (LAMMP) NIH grant P41 RR01192; the U.S. Air Force Office of Scientific Research, Medical Free-Electron Laser Program (F49620-00-2-0371 and FA9550-04-1-0101); The Beckman Foundation; ASLMS Student Travel Grant.

Contract grant sponsor: Laser Microbeam and Medical Program (LAMMP) NIH; Contract grant number: P41 RR01192; Contract grant sponsor: U.S. Air Force Office of Scientific Research, Medical Free-Electron Laser Program; Contract grant numbers: F49620-00-2-0371, FA9550-04-1-0101; Contract grant sponsor: The Beckman Foundation; Contract grant sponsor: ASLMS Student Travel Grant.

References

1. Laumann AE, Derick AJ. Tattoos and body piercings in the United States: A national data set. J Am Acad Dermatol 2006;55(3):413–421. [PubMed: 16908345]
2. Sweeney SM. Tattoos: A review of tattoo practices and potential treatment options for removal. Curr Opin Pediatr 2006;18(4):391–395. [PubMed: 16914993]
3. Tanzi EL, Lupton JR, Alster TS. Lasers in dermatology: Four decades of progress. J Am Acad Dermatol 2003;49(1):1–31. [PubMed: 12833005]quiz 31–34
4. Handley JM. Adverse events associated with nonablative cutaneous visible and infrared laser treatment. J Am Acad Dermatol 2006;55(3):482–489. [PubMed: 16908355]
5. Ross EV, et al. Tattoo darkening and nonresponse after laser treatment: A possible role for titanium dioxide. Arch Dermatol 2001;137(1):33–37. [PubMed: 11176658]
6. Haedersdal M, Bech-Thomsen N, Wulf HC. Skin reflectance-guided laser selections for treatment of decorative tattoos. Arch Dermatol 1996;132(4):403–407. [PubMed: 8629843]
7. Cerussi A, et al. In vivo absorption, scattering, and physiologic properties of 58 malignant breast tumors determined by broadband diffuse optical spectroscopy. J Biomed Opt 2006;11(4):044005. [PubMed: 16965162]

8. Bevilacqua F, et al. Broadband absorption spectroscopy in turbid media by combined frequency-domain and steady-state methods. Appl Opt 2000;39(34):6498–6507. [PubMed: 18354663]
9. Baumler W, et al. Q-switch laser and tattoo pigments: First results of the chemical and photophysical analysis of 41 compounds. Lasers Surg Med 2000;26(1):13–21. [PubMed: 10636999]
10. Beute TC, et al. In vitro spectral analysis of tattoo pigments. Dermatol Surg 2008;34(4):508–515. [PubMed: 18248489]discussion 515–516
11. O'Goshi K, Suihko C, Serup J. In vivo imaging of intradermal tattoos by confocal scanning laser microscopy. Skin Res Technol 2006;12(2):94–98. [PubMed: 16626382]
12. Cuccia DJ, et al. Quantitation and mapping of turbid media optical properties using modulated imaging. J Biomed Opt. 2009in press
13. Neil MAA, Juskaitis R, Wilson T. Method of obtaining optical sectioning by using structured light in a conventional microscope. Opt Lett 1997;22(24):1905–1907. [PubMed: 18188403]
14. Carlson, AB.; Crilly, PB.; Rutledge, JC. McGraw-Hill Series in Electrical and Computer Engineering. Vol. 4th. Vol. xiii. Boston: McGraw-Hill; 2002. Communication systems: An introduction to signals and noise in electrical communication; p. 850
15. Yoon G, Prahl A, Welch AJ. Accuracies of the diffusion approximation and its similarity relations for laser irradiated biological media. Appl Opt 1989;28(12):2250–2255.
16. Pogue BW, et al. Image analysis methods for diffuse optical tomography. J Biomed Opt 2006;11(3): 33001. [PubMed: 16822050]
17. Ayers, F., et al. Design and Performance Validation of Phantoms Used in Conjunction with Optical Measurements of Tissue. San Jose, CA USA: SPIE; 2008. Fabrication and characterization of silicone-based tissue phantoms with tunable optical properties in the visible and near infrared domain.
18. Haskell RC, et al. Boundary conditions for the diffusion equation in radiative transfer. J Opt Soc Am A Opt Image Sci Vis 1994;11(10):2727–2741. [PubMed: 7931757]
19. Swartling J, et al. Accelerated Monte Carlo models to simulate fluorescence spectra from layered tissues. J Opt Soc Am A Opt Image Sci Vis 2003;20(4):714–727. [PubMed: 12683499]
20. Tseng SH, Grant A, Durkin AJ. In vivo determination of skin near-infrared optical properties using diffuse optical spectroscopy. J Biomed Opt 2008;13(1):014016. [PubMed: 18315374]
21. Timko AL, et al. In vitro quantitative chemical analysis of tattoo pigments. Arch Dermatol 2001;137 (2):143–147. [PubMed: 11176685]
22. Weber JR, et al. Non-contact imaging of absorption and scattering in layered tissue using spatially-modulated structured light. Appl Phys. 2009in press

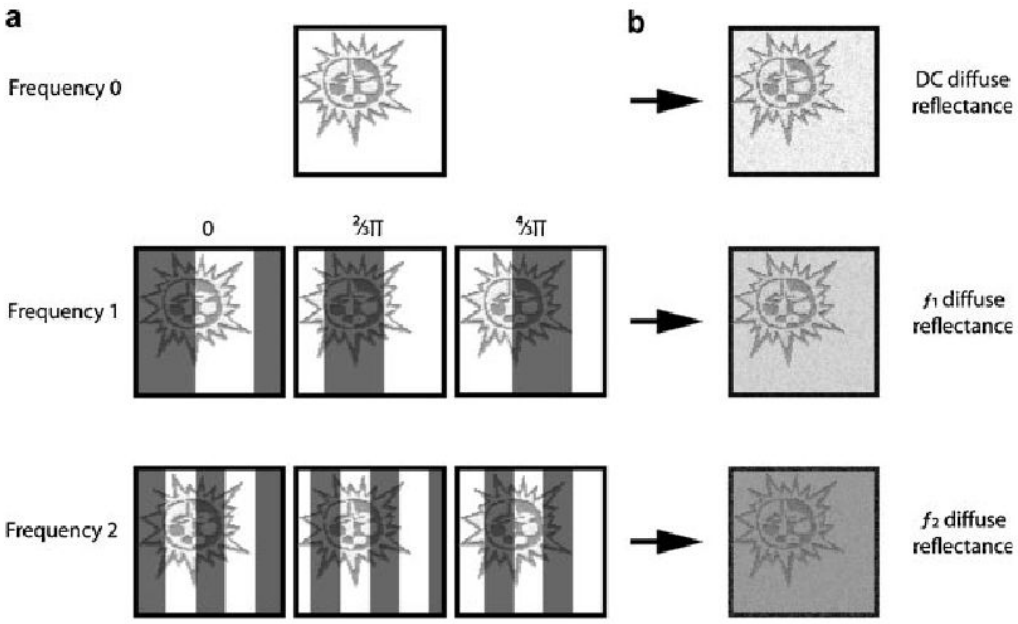

Fig. 1.

The MI instrument field of view. **a:** A tattoo is illuminated with planar light at Frequency 0. Frequency 1 shows the tattoo illuminated with a spatial sine wave pattern that is phase shifted 120° as you move from the leftmost image to the rightmost image. Frequency 2 shows a similar image set with a higher frequency sine wave pattern. **b:** The three phase shifted patterns are demodulated to form a map of frequency dependent, non-modulated diffuse reflectance similar to the map of diffuse reflectance generated with planar illumination.

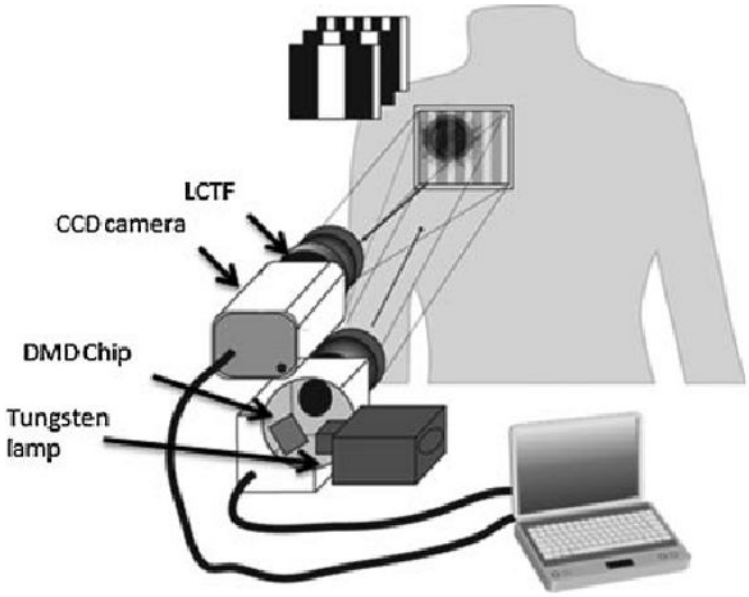

Fig. 2.

Diagram of the modulated imaging system. Light generated by a Tungsten lamp is directed onto the digital micro-mirror device (DMD) chip which generates the spatial frequency patterns. These patterns are projected directly onto the region of interest on the subject and the diffuse reflectance is captured at discrete wavelengths by the CCD camera and incorporated liquid crystal tunable filter (LCTF).

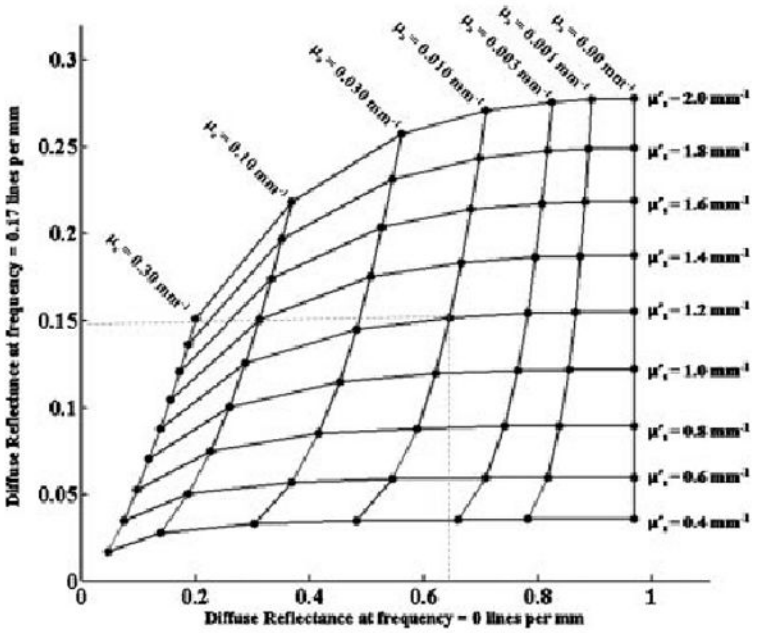

Fig. 3.

A graphical representation of the Monte–Carlo generated look-up table. The center grid is made up of horizontal lines marking absorption values (μ_a) decreasing from left to right, and vertical lines marking reduced scattering values (μ'_s) decreasing from top to bottom. Each intersection represents a unique combination of absorption and reduced scattering and has a particular diffuse reflectance value for the non-modulated light on the *x*-axis and the modulated light on the *y*-axis.

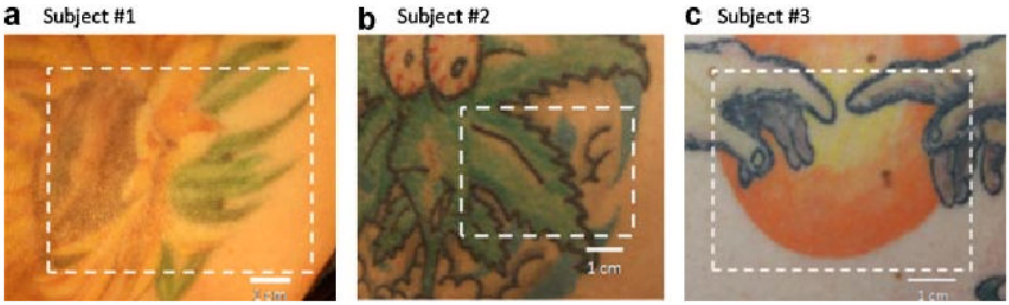

Fig. 4.

Three tattoos investigated with the modulated imaging system: (**a**) A sunflower tattoo featuring green, orange, and burnt-red colors, (**b**) a green leaf tattoo feature green and blue colors, (**c**) a sun tattoo featuring yellow and orange colors. The field-of-view used for each tattoo is outlined by the dashed line.

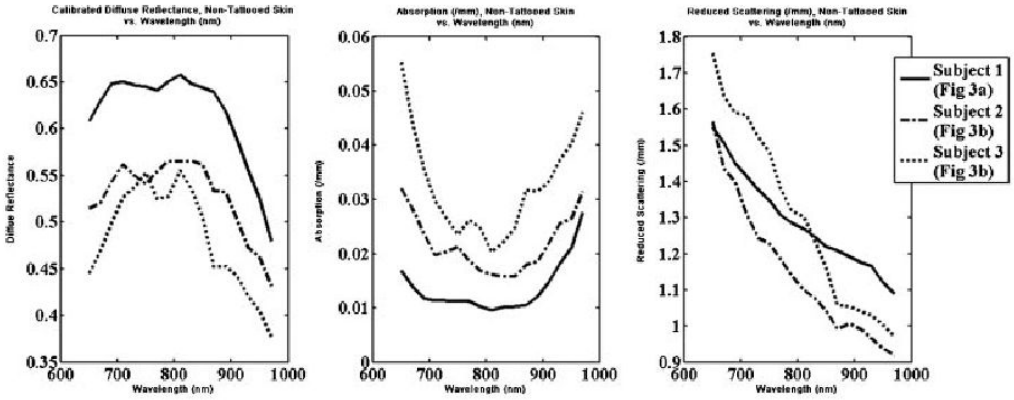

Fig. 5.

Mean optical properties for non-tattooed skin of each subject. From left to right: The calibrated unmodulated diffuse reflectance, the mean recovered absorption coefficient, and the mean reduced scattering coefficient.

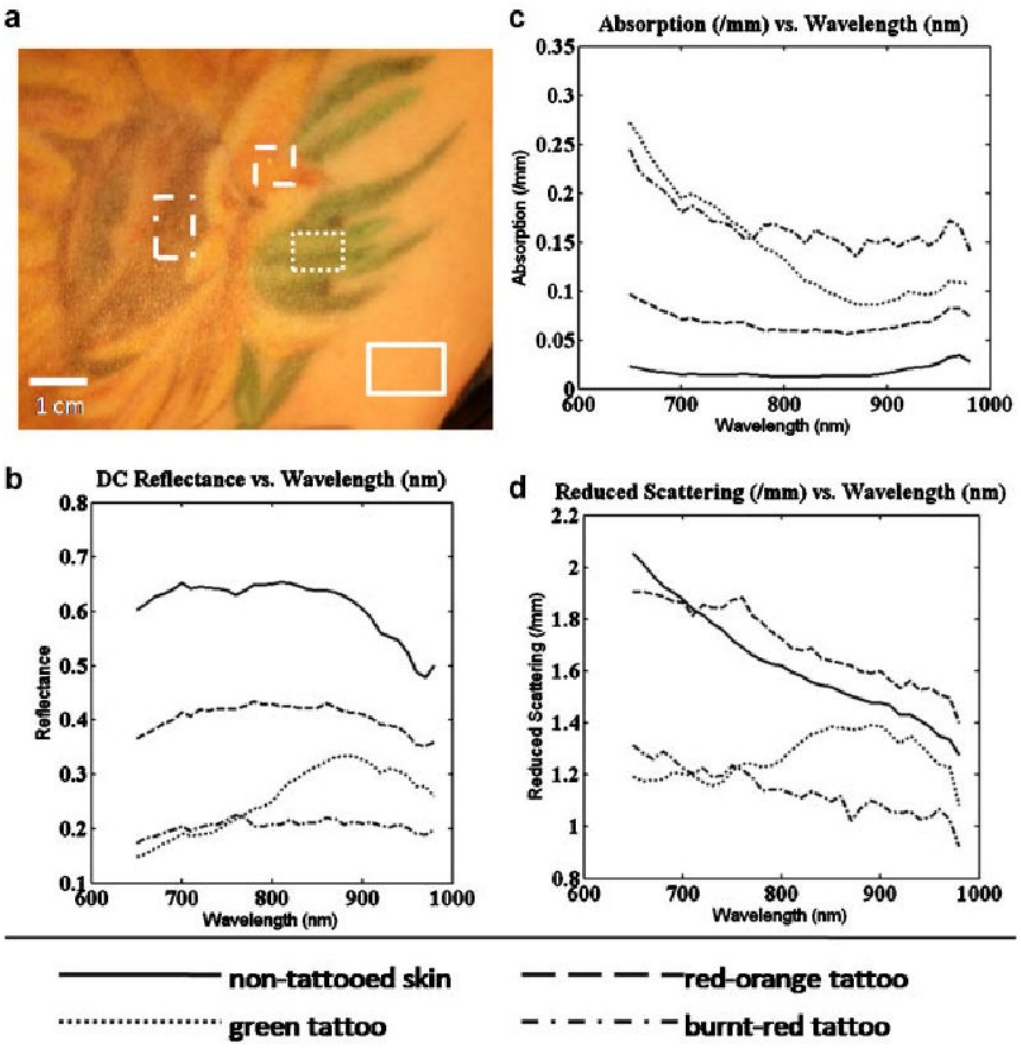

Fig. 6.

Mean optical properties for selected regions of interest, Subject #1. **a:** Color photo of tattoo with selected regions of interest highlighted. **b:** Unmodulated diffuse reflectance. **c:** Mean recovered absorption coefficients. **d:** Mean recovered reduced scattering coefficients.

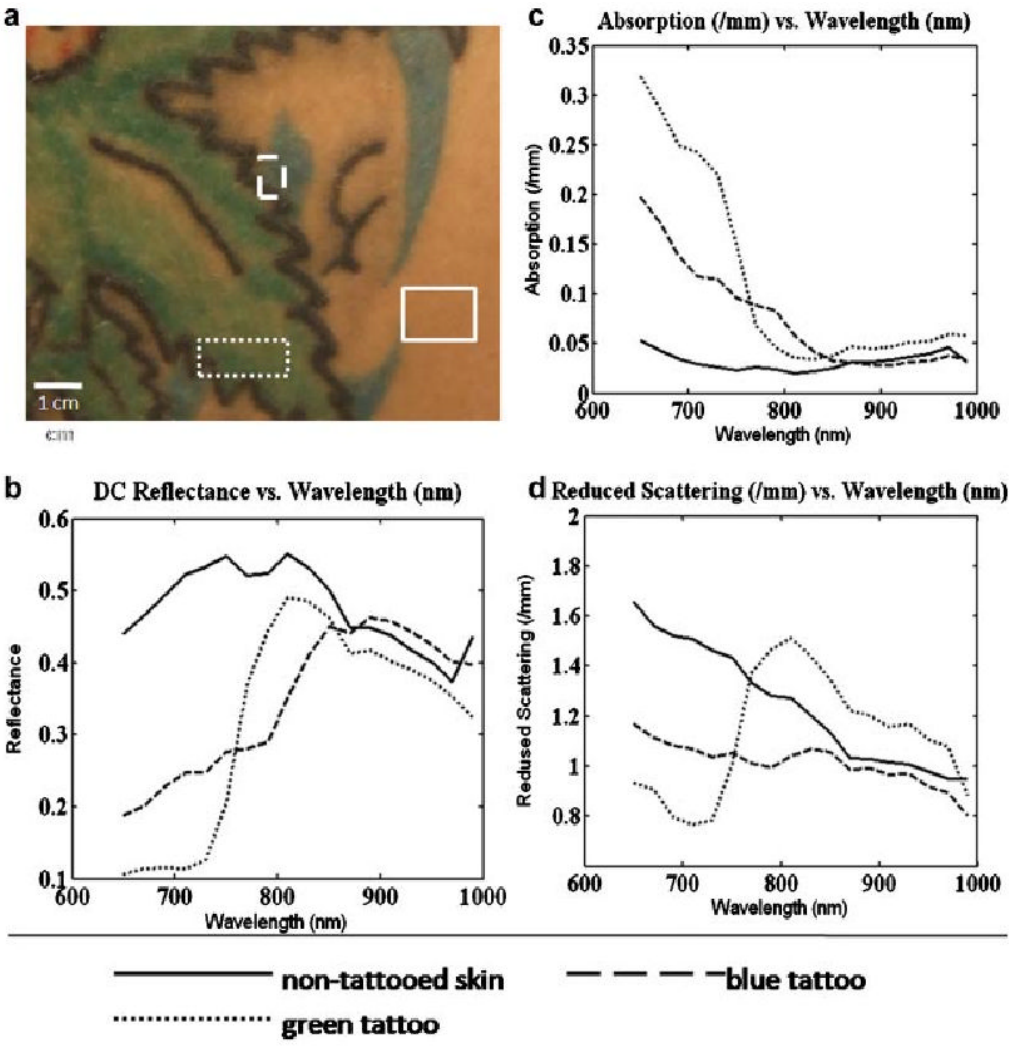

Fig. 7.

Mean optical properties for selected regions of interest, Subject #2. **a:** Color photo of tattoo with selected regions of interest highlighted. **b:** Unmodulated diffuse reflectance. **c:** Mean recovered absorption coefficients. **d:** Mean recovered reduced scattering coefficients.

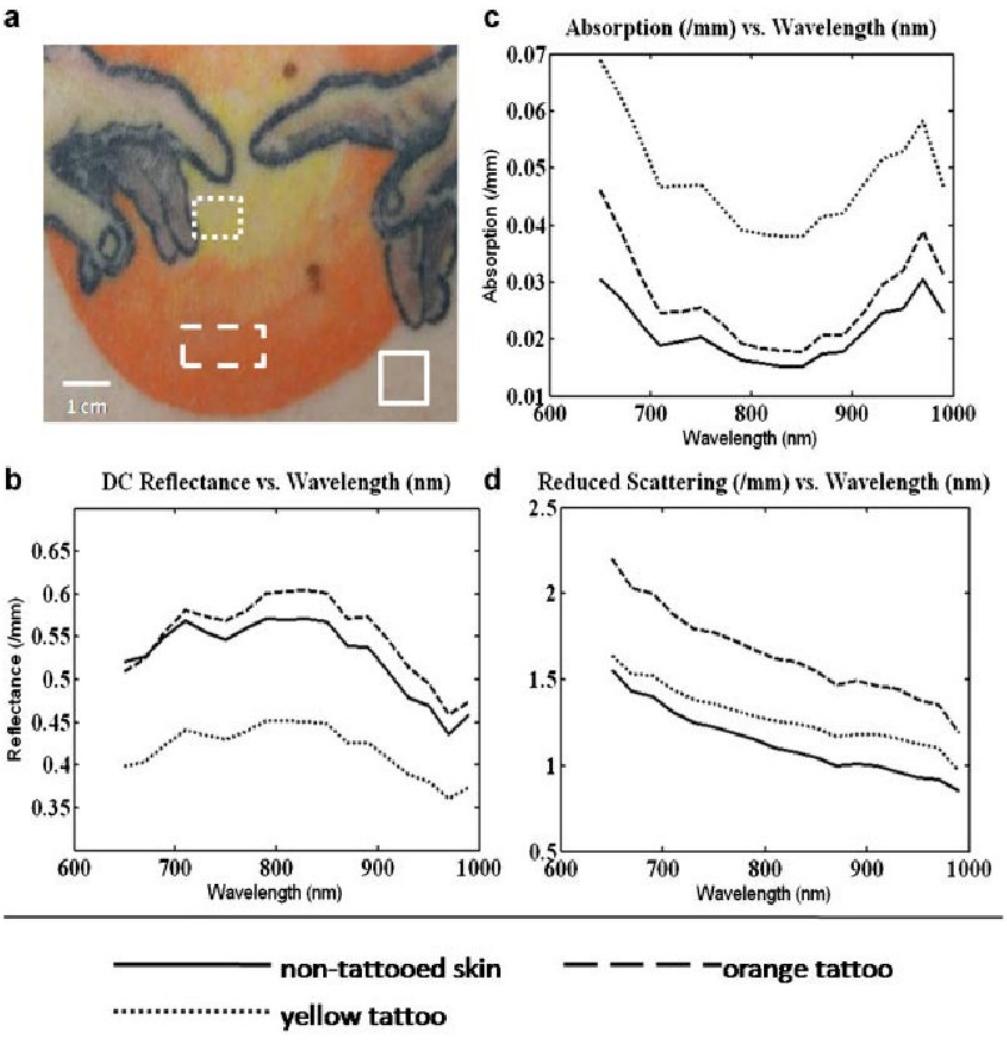

Fig. 8.

Mean optical properties for selected regions of interest, Subject #3. **a:** Color photo of tattoo with selected regions of interest highlighted. **b:** Unmodulated diffuse reflectance. **c:** Mean recovered absorption coefficients. **d:** Mean recovered reduced scattering coefficients.

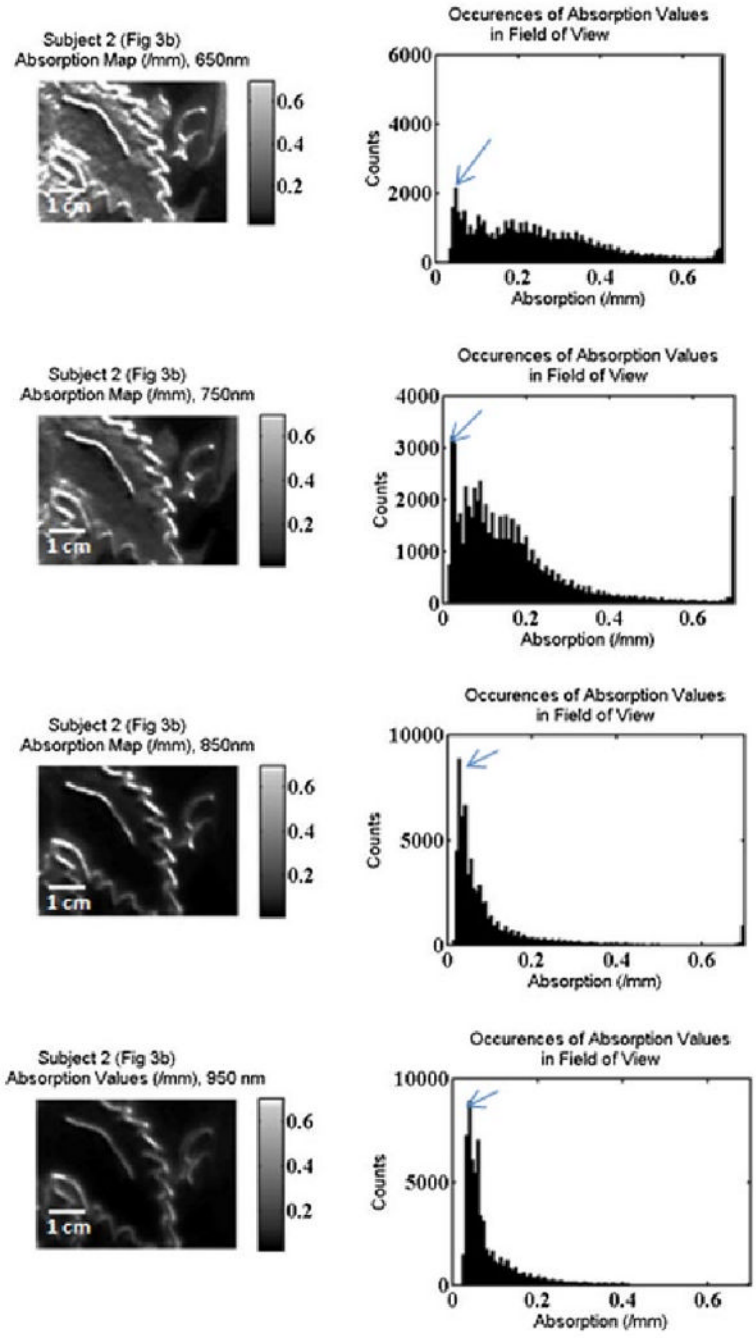

Fig. 9.

2-D false color, grayscale absorption map and accompanying histogram, showing from top to bottom: 650, 750, 850, 950 nm. The arrow points to the bin that includes the recovered mean absorption value of the non-tattooed skin.

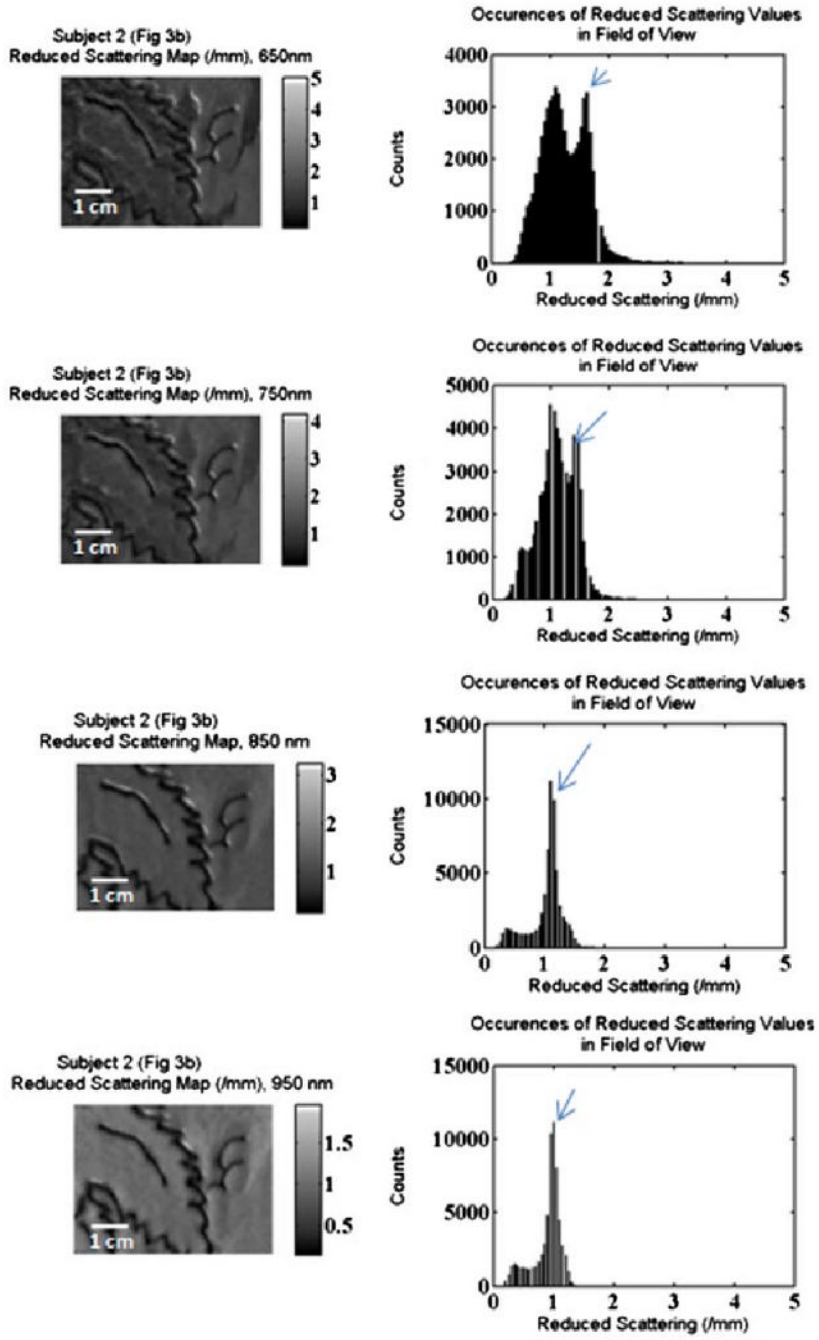

Fig. 10.

2-D false color, grayscale reduced scattering map and accompanying histogram, showing from top to bottom:650, 750, 850, 950 nm. The arrow points to the bin that includes the recovered mean reduced scattering value of the non-tattooed skin.

TABLE 1
Parameters of the Monte–Carlo Generated Lookup Table

Lookup table parameters	
Number points, μ_a	349
Min μ_a	0.003 mm^{-1}
Max μ_a	0.70 mm^{-1}
Number points, μ_s'	138
Min μ_s'	0.15 mm^{-1}
Min μ_s'	7.0 mm^{-1}

Diffuse reflectance values were calculated for each of the frequencies at every combination of the 349 absorption coefficients (μ_a) and 138 reduced scattering coefficients (μ_s'). Because the optical properties of in vivo tattooed skin have not been fully characterized, a large range of absorption and reduced scattering values were incorporated.